Article

Hydrogen Storage Characteristics and Corrosion Behavior of V-rich Ti-V-Cr-Fe Alloy

Jimoh Mohammed Abdul [1,2,*], Lesley Hearth Chown [1], Jamiu K. Odusote [3], Jean Nei [4], Kwo-Hsiung Young [4] and Woli Taiye Olayinka [2]

[1] School of Chemical and Metallurgical Engineering, Faculty of Engineering and Built Environment, University of the Witwatersrand, Johannesburg Private Bag 3, Wits 2050, South Africa; Lhchown@gmail.com

[2] Department of Mechanical Engineering, Faculty of Engineering, Federal Polytechnic, Offa, Nigeria; taiyewoli@gmail.com

[3] Department of Metallurgy and Material Science, Faculty of Engineering University of Ilorin, Nigeria; jamiukolawole@gmail.com

[4] BASF/Battery Materials-Ovonic, 2983 Waterview Drive, Rochester Hills, MI 48309, USA; jean.nei@basf.com (J.N.); kwo.young@basf.com (K.Y)

* Correspondence: jmabdul@gmail.com or jmabdul66@yahoo.com; Tel.: +1-234-805-562-9924; +234-090-848-80106

Abstract: In this work, we investigated the effects of heat treatment on the microstructure, hydrogen storage characteristics and corrosion rate of a $Ti_{34}V_{40}Cr_{24}Fe_2$ alloy. The arc melted alloy was divided into three samples, two of which were separately quartz-sealed under vacuum and heated to 1000 °C for 1 h; one of these samples was quenched and the other furnace cooled to ambient temperature. The crystal structures of the samples were studied via X-ray diffractometry and scanning electron microscopy. Absorption/desorption characteristics were investigated using a Sievert apparatus. Potentiostat corrosion tests on the alloys were performed using an AutoLab® corrosion test apparatus and electrochemical cell. All samples exhibited a mixture of body-center-cubic (BCC) and Laves phase structures. The corrosion rate, maximum absorption, and useful capacities increased after both heat treatments. The annealed sample had the highest absorption and reversible capacity. The plateau pressure of the as-cast alloy increased after quenching. The corrosion rate increased from 0.0004 mm/y in as-cast sample to 0.0009 mm/y after annealing and 0.0017 mm/y after quenching, due to a decrease in the Cr-content of the C14 phase.

Keywords: Ti-V-Cr-Fe alloy; hydrogen storage characteristics; metal corrosion; heat treatment; crystal structure

1. Introduction

Ti-V-Cr body-centered-cubic (BCC) solid solution alloys are very promising to store a large quantity of hydrogen at room temperature [1–3]. Some of the identified shortcomings of these alloys include poor pressure-concertation-temperature (PCT) plateau characteristics, low hydrogen desorption capacities, and long activation times [4–7]. In an attempt to improve on these shortcomings, controlled quantities of additives such as Fe, Zr and Mn have been found to be effective in lowering cost and enhancing the overall performance of the alloy [8–11]. Further efforts include assessing the effects of heat treatment on hydrogen absorption properties; Okada *et al*. [1] found that moderate heat treatment, specifically annealing at 1573 K for 1 min, enhances the storage capacity and flattens the desorption plateau of $Ti_{25}Cr_{40}V_{35}$ alloy. Liu *et al*. [12] reported that heat treatment effectively improves the flatness of plateau and improves the hydrogenation capacity of $Ti_{32}Cr_{46}V_{22}$ alloy by lowering the oxygen concentration and homogenizing the composition and microstructure. A hydrogen desorption capacity of 2.3 wt% was achieved when $Ti_{32}Cr_{40}V_{25}$ was annealed at 1653 K for 1 min. [13]. Chuang *et al*. [14] found that annealing atomized powder of Ti-Zr

based alloy at 1123 K for 4 h greatly enhanced the discharge capacity. Hang *et al*. [15] heat treated $Ti_{10}V_{77}Cr_6Fe_6Zr$ alloy at a relatively lower temperature, but elongated the soaking time by annealing at 1523 K for 5 min and at 1373 K for 8 h and found that sample annealed at 1523 K for 5 min has the best overall hydrogen storage properties, with a desorption capacity of 1.82 wt% and a dehydriding plateau pressure of 0.75 MPa.

Although BCC solid solution alloys have very high gaseous phase hydrogen storage capacities, they suffer from the severe capacity degradation during electrochemical applications due to leaching-out of Vanadium (V) into the KOH electrolyte [16,17]. The preferential leaching of V in the negative electrode material has been previously identified [18] and V-free Laves phase alloys have been adopted to mitigate the consequent cycle life and self-discharge issues originating from V-corrosion [19,20]. Metal corrosion mainly occurs through electrochemical reactions at the interface between the metal and electrolyte [21]. The rate of the reaction is evaluated in terms of the corrosion current. The natural logarithm of the absolute value of the corrosion current versus potential is plotted as a Tafel curve. The corrosion current values can be transformed to corrosion rate (*CR*) values (e.g. mm/y) using Equation 1 [22]:

$$CR = K \frac{i_{corr}}{\rho} EW, \quad (1)$$

where K is a constant that depends on the unit of corrosion rate; K = 3272 for mm/y (mmpy), or = 1.288 x 10^5 for milli-inches/y (mpy), i_{corr} = corrosion current density, μA Cm^{-2}, ρ = alloy density. EW = Equivalent weight = 1/electron equivalent (Q) where:

$$Q = \sum \frac{n_i f_i}{W_i}, \quad (2)$$

where n_i = the valence if i^{th} element of the alloy, f_i = the mass fraction of the i^{th} element in the alloy, Wi = the atomic weight of the i^{th} element in the alloy.
By combining Equations 1 and 2, the penetration rate (*CR* and mass loss, *ML*) of an alloy is given by:

$$CR = K_1 \frac{i_{corr}}{\rho \sum \frac{n_i f_i}{W_i}} \quad (3)$$

$$ML = K_2 i_{corr} EW \quad (4)$$

The equations above give values of 0.1288 if the unit of CR is m/y and 0.03272 if the unit of CR is mm/y [21]. This work investigates the influence of heat treatment on hydrogen storage capacity and corrosion rate of $Ti_{34}V_{40}Cr_{24}Fe_2$ in standard KOH electrolyte. V-based hydrogen storage alloys are often used as the anode in NiMH batteries [23]. Hence, there is a need to investigate the corrosion behavior of V in such alloys.

2. Experimental Setup

10g sample of $Ti_{34}V_{40}Cr_{24}Fe_2$ alloy was prepared in a water-cooled, copper-crucible arc melting furnace under argon atmosphere. The ingot was turned over and remelted three times to ensure homogeneity. After melting, the ingot was divided into three pieces. Two cut samples were vacuum-sealed in separate silica glass tubes in preparation for heat treatment.

The two quartz-sealed specimens were loaded in a heat treatment furnace and heated to 1000 °C for 1 h. One tube was immediately removed and broken in cold water to quench the alloy,thereby locking the microstructure, while the second sample was slowly furnace-cooled to room temperature.

Crystal structure and lattice parameters in the as-cast and heat-treated samples were determined by X-ray diffraction (XRD) analysis, using a Bruker D2_Phaser X-ray® diffraction instrument (Bruker AXS, Inc., Madison, Wisconsin, USA) with Cu-K_α radiation from 2θ = 10° to 80°. Elemental compositions of the phases were determined using a FEI Nova NanoSEM 200® scanning

Preprints (www.preprints.org) | NOT PEER-REVIEWED | Posted: 31 March 2017 doi:10.20944/preprints201703.0228.v1

Peer-reviewed version available at Batteries 2017, 3, , 19; doi:10.3390/batteries3020019

electron microscope (SEM) (FEI, Hillsboro, Oregon, USA) fitted with EDAX® advanced microanalysis solution (EDAX Inc., Mahwah, New Jersey, USA). The amount of the phases was determined by image analysis using the ImageJ freeware (National Institute of Mental Health, Bethesda, Maryland, USA).

Pottentiostatic corrosion tests on the alloys were performed using an AutoLab® corrosion test apparatus (Metrohm Autolab B.V., Utrecht, The Netherlands) and an electrochemical cell consisting of a tri-electrode; platinum reference electrode, Ag/AgCl counter electrode, and test alloy as the working electrode; aqueous solution of 6 mol L^{-1} KOH was used as the electrolyte. The alloys were cut into rectangles and a copper wire of suitable length was attached to one side of the specimen with aluminum tape. The sample was then covered in cold-resin for 24 h to enable curing, while leaving only the test surface exposed. When cured, the test surface was ground to 120 grit. The corrosion experiments were performed at 25 °C and Tafel curves were recorded from –1.4V to –0.2 V with a scanning rate of 1 mV sec^{-1}.

Measurement of the PCT isotherms was performed using a Sieverts-type apparatus. Samples were crushed into particles < 75 μm in size and 1g of each alloy was sealed into a stainless steel reactor and heated to 573 K. Next, 3 MPa of Hydrogen pressure was introduced into the apparatus for 30 min, followed by slow cooling to room temperature in a hydrogen atmosphere. The alloys absorbed most of the hydrogen and were pulverized in this step. After the absorption process, the samples were heated to 573 K and chamber was evacuated for 1 h with a mechanical pump to completely dehydrogenate the samples for PCT measurements at 303, 333, and 363 K successively.

3. Results and discussion

3.1. Microstrcuture

Figure 1 shows representative back scattering electron (BSE) images of as-cast and heat treated (both slow cooled and quenched) $Ti_{34}V_{40}Cr_{24}Fe_2$. Addition of Fe into the TiVCr solid solution is known to promote the secondary Laves phase [24–26], which is considered to be a catalyst that facilitates hydrogen absorption/desorption kinetics [27]. The microstructure of the alloy was a primary, light grey phase (C) with a black intergranular phase (D) in all three samples. In addition, a dark grey intergranular phase (E) was observed in the as-cast sample and this phase exhibited a different composition from D. X-ray energy dispersive spectroscopy (EDS) analyses on the dark portions (E) on the micrographs of annealed samples have the same elemental compositions as those in the Laves phase. The XRD pattern in Figure 2 shows that the primary light grey phase corresponds to the main peak of BCC (V) phase, while the black intergranular and the dark phases were the minor peaks of the C14 Laves phase. Annealing removed the dark grey Laves phase, while quenching increased the proportion of the phase from 1.3 to 32.5%. Quenching introduced twinning in the secondary Laves phase, shown inside the circle (F). Reduction in the C14 secondary phase abundance by thermal annealing was also reported before with a Laves phase-related BCC TiZrV-based alloy [28].

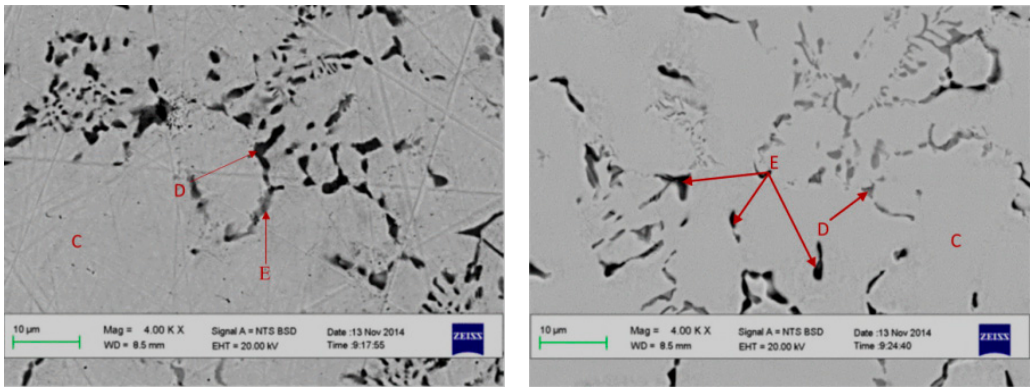

(**a**) (**b**)

Preprints (www.preprints.org) | NOT PEER-REVIEWED | Posted: 31 March 2017 doi:10.20944/preprints201703.0228.v1

Peer-reviewed version available at Batteries 2017, 3, , 19; doi:10.3390/batteries3020019

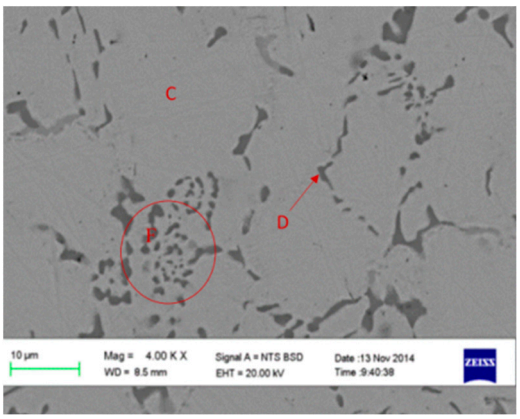

(**c**)

Figure 1. SEM BSE micrographs of (**a**) as-cast, (**b**) annealed, and (**c**) quenched $Ti_{34}V_{40}Cr_{24}Fe_2$.

Table 1 demonstrates that the BCC (V) in all the three samples contained 17–22 at% Ti, 40–44 at% V, and ~36 at% Cr. The black intergranular C14 Laves phase contained 23–66 at% Ti, 18–41 at% V, and 14–36 at% Cr. The annealing treatment removed the dark grey C14 Laves (unit cell volume 161.7 $Å^3$), while quenching dissolved the Laves phase with a smaller unit cell volume. The Ti/Cr ratio in the BCC phase is almost equal in all three samples. However, the ratio of the Laves phase increased from 0.6 to 4.4 after annealing and ~2 after quenching.

Table 1. **EDX and crystallographic parameters of as-cast and heat treated $Ti_{34}V_{40}Cr_{24}Fe_2$.**

Sample	Phases XRD	Composition (at%)				Ti/Cr ratio	Phase proportion (% area)	Crystallographic description			
		Ti	V	Cr	Fe			Space group (no.)	*a*	*c*	Unit cell vol. ($Å^3$)
As-cast	BCC (V)	17.7 (1.1)	43.5 (1.6)	36.5 (2.2)	2.3 (0.7)	0.5	78.5	$Im\bar{3}m$ (229)	3.00		27.08
	C14 (Laves)	23.0 (3.7)	41.4 (2.4)	35.5 (1.4)	2.0 (0.2)	0.6	20.2	$P6_3/mmc$ (194)	2.98	4.73	36.24
	C14 (Laves)	24.7 (0.8)	37.8 (0.7)	34.0 (0.4)	3.5 (0.3)	0.7	1.3	$P6_3/mmc$ (194)	4.85	7.94	161.7
Annealed	BCC (V)	17.7 (1.9)	43.5 (1.3)	36.5 (2.9)	2.3 (0.2)	0.5	82.0	$Im\bar{3}m$ (229)	3.01		27.37
	C14 (Laves)	65.9 (5.2)	18.6 (2.8)	14.9 (2.2)	0.6 (0.2)	4.4	18.0	$P6_3/mmc$ (194)	2.98	4.73	36.24
Quenched	BCC (V)	21.8 (1.5)	40.0 (1.3)	35.6 (1.2)	2.6 (1.7)	0.6	67.5	$Im\bar{3}m$ (229)	3.01		27.37
	C14 (Laves)	47.3 (3.7)	21.6 (2.5)	24.7 (1.4)	6.4 (0.5)	1.9	32.5	$P6_3/mmc$ (194)	4.85	7.94	161.7

Table 1 shows that the proportion of the BCC (V) phase in as-cast sample was ~79% area-wise. The dark phase and light grey C14 Laves phases made up approximately 20% and 1.3%, respectively, of the total alloy. Annealing had no effect on the composition of the BCC phase, but increased the proportion of BCC phase to 82%. Quenching reduced the proportion of BCC by 11% and increased Ti-content by ~4 at%. Proportion of the Laves phase was slightly reduced from 20% in the as-cast sample to 18% in the annealed sample, but increased to 32.5% after quenching.

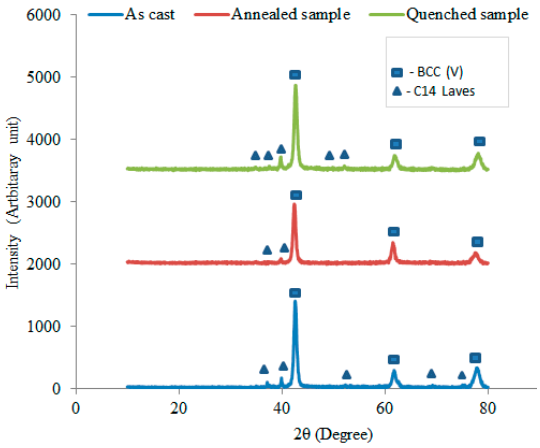

Figure 2. XRD patterns of as-cast and heat treated $Ti_{34}V_{40}Cr_{24}Fe_2$ alloys.

3.2 Gaseous phase hydrogen storage

Table 2 shows that both heat treatment processes increased the reversible hydrogen storage capacity (RHSC), the capacity increased from 0.44 to 1.26 wt% after annealing and to 1.26 wt% in quenched the sample. The literature indicates that annealing increases hydrogen capacity [13,14]. The BCC phase enhances hydrogen capacity [11,22,29]; increases in the unit cell volume implies the availability of more hydrogen absorption sites or spaces, leading to an increase in storage capacity. The Laves phase is detrimental to storage capacity [10,30–32], and alloys with larger Laves unit cell volumes or high Laves proportions are known to exhibit lower hydrogen capacity. Therefore, the observed increase in useful capacity after heat treatment was due to the increase in BCC unit cell volume. The larger unit cell volume of the Laves phase in the as-cast sample disappeared after annealing; this suggests another reason for the higher hydrogen capacity observed in the annealed sample.

Table 2 also shows that the plateau pressure reduced after annealing and rose after quenching. Specifically, the pressure of the plateau decreased from 1.32 to 0.68 MPa after annealing and increased to 2.34 MPa after quenching. The plateau properties are affected by both the homogeneity and oxygen content in Ti-V based hydrogen storage alloys [10]. Inhomogeneity of microstructure can be minimized by heat treatment at higher temperatures for a short time [33]. The observed reduction in plateau pressure after annealing suggest a homogenized microstructure; in addition, the sample was annealed in a vacuum-sealed quartz tube, thereby preventing oxygen intake. The quenched sample was exposed to oxygen in the quenching medium; therefore, the rise in plateau pressure suggests the presence of a higher oxygen content.

Table 2. Effect of heat treatment on H storage properties of $Ti_{34}V_{40}Cr_{24}Fe_2$ alloy

Sample	Absorption capacity (wt%)	Capacity remaining (wt%)	RHSC (wt%)	Plateau pressure (MPa)
As-cast	0.86	0.42	0.44	1.32
Annealed	1.54	0.28	1.26	0.68
Quenched	1.04	0.39	0.65	2.34

In Figure 3a, the PCT isotherms for both the as-cast and heat treated alloys were steep, an indication of high plateau pressure. However, the isotherm for the annealed sample showed a flatter and wider plateau, indicating a reduction in plateau pressure, and the wider plateau indicating higher hydrogen capacity.

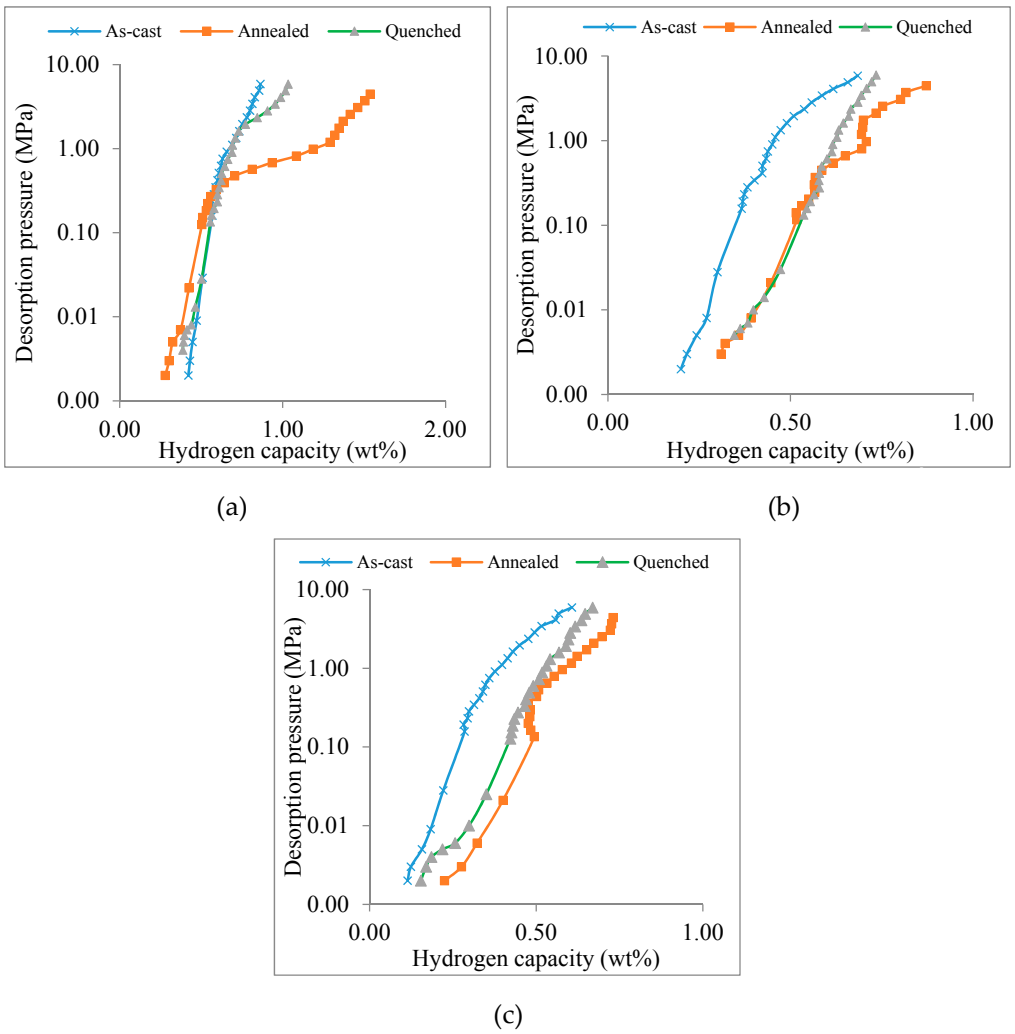

Figure 3. PCT desorption curves of the as-cast and heat treated $Ti_{34}V_{40}Cr_{24}Fe_2$ alloys at (**a**) 303, (**b**) 333, and (**c**) 363 K.

In Figure 4, the maximum absorption capacity decreased with increasing isotherm temperatures, similar to what has previously been described in the literature [34]. For the as-cast sample, the maximum absorption capacity was 0.86 wt% at 30 °C, and the capacity declined to 0.69 and 0.62 wt% as the temperature rose to 333 and 363 K, respectively. Similar trends were observed for the annealed and quenched samples. Kinetic energy of gas increased with increasing temperatures; a low kinetic energy is associated with lower temperatures, while increased temperature leads to high kinetic energy. Hydrogen gas atoms with a low kinetic energy are more easily absorbed than those with high kinetic energy because gases with higher kinetic energy move faster, thus requiring additional force to attract to the surface of the adsorbate. This explains the observed higher capacity at low temperatures and lower capacity at high temperatures.

Preprints (www.preprints.org) | NOT PEER-REVIEWED | Posted: 31 March 2017 doi:10.20944/preprints201703.0228.v1

Peer-reviewed version available at Batteries 2017, 3, , 19; doi:10.3390/batteries3020019

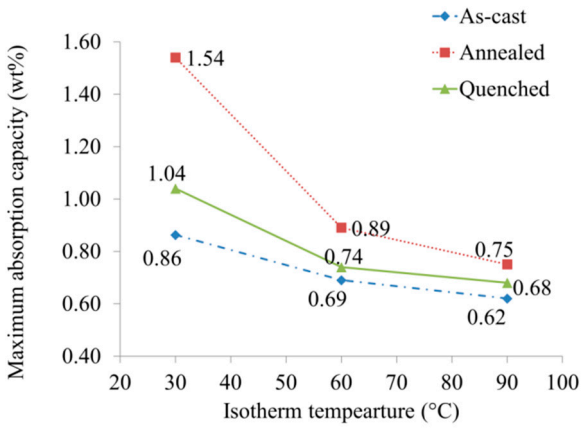

Figure 4. Influence of isotherm temperatures on maximum hydrogen capacity.

3.3 Corrosion behavior

The corrosion behavior of $Ti_{34}V_{40}Cr_{24}Fe_2$ alloys with different preparations in 30% KOH aqueous solution was studied by Tafel curve measurements and results are plotted in Figure 5a. No significant change was observed in corrosion potential (E_{corr}) for the as-cast alloy after annealing. However, a decrease from –0.80 to –0.867 mV was observed after quenching. Both heat treatment processes increased the corrosion rate of the alloy (Figure 5b). The rate increased from 0.0004 in as-cast alloy to 0.0009 mm/y after annealing and to 0.0017mm/y after quenching.

Cr is known to improve the corrosion resistance of an alloy [35,36]. Samples containing high at% Cr are expected to have low corrosion rates and vice versa. Therefore, an increase in the corrosion rate of heat treated samples could be a result of a reduction in Cr-content in the C14 secondary phase. Phase structure and oxide layer are among the factors that determine the corrosion rate of an alloy. The Laves structure have been reported to have a thinner oxide layer than the BCC structure [11] and this oxide layer is known for passivation of corrosion [37–39]. It is therefore implied that for a dual phase alloy, like the alloys being investigated in this research, the corrosion rate will increase when the proportion of Laves phase with thinner oxide layer increases. The Laves phase was introduced before to facilitate the formation process [40,41], and then is more easily corroded than the BCC phase. The high Laves phase proportion in the quenched sample therefore suggests the basis for the observed increase in corrosion rate.

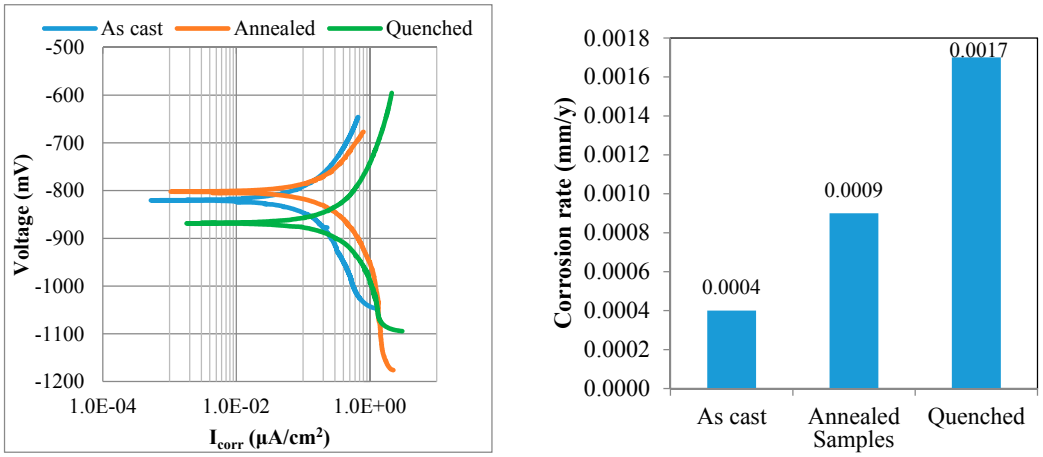

(**a**) (**b**)

Figure 5. (**a**) Tafel curves and (**b**) corrosion rates of the as-cast and heat treated $Ti_{34}V_{40}Cr_{24}Fe_2$.

4. Conclusions

The influence of heat treatment on the microstructure and hydrogen storage capacity of $Ti_{34}V_{40}Cr_{24}Fe_2$ at% alloys was investigated. Both the as-cast and heat treated samples contained BCC and Laves phases. Heat treatment was beneficial with regard to hydrogen capacity, but detrimental to corrosion behavior. Though both heat treatment processes enhanced useful hydrogen capacity, the annealed sample had superior storage characteristics. Although both annealing and quenching increased the corrosion rate of the alloy, the rate of corrosion was found to be highest in the quenched sample. For electrochemical applications, annealing of a BCC-based metal hydride must be controlled in a manner that does not overly reduce the Cr-content in the C14 phase in order to minimize the corrosion rate.

Acknowledgments: The work is supported by African Material Science and Engineering Network, AMSEN, and the National Research Found NRF Thuthuka programme.

Author Contributions: Jimoh Mohammed Abdul and Lesley Hearth Chown designed the experiments and analyzed the results. Jamiu K. Odusote and Jean Nei conducted the corrosion and PCT measurements, respectively, and Kwo-Hsiung Young and Woli T. Olayinka, assisted in data analysis and manuscript preparation.

Conflicts of Interest: The authors declare no conflict of interest.

Abbreviations

BCC	Body-centered-cubic
PCT	Pressure-concentration-temperature
CR	Corrosion rate
i_{corr}	Corrosion current density
EW	Equivalent weight
ML	Mass loss
XRD	X-ray diffractometer
SEM	Scanning electron microscopy
BSE	Back-scattering electron
EDS	Energy dispersive spectroscopy
RHSC	Reversible hydrogen storage capacity
E_{corr}	Corrosion potential

References

1. Okada, M.; Kuriiwa, T.; Tamura, T.; Kamegawa, A. Ti-V-Cr b.c.c. alloys with high protium content. *J. Alloys Compd.* **2002**, *330–332*, 511–516.
2. Tamura, T.; Kazumi, T.; Kamegawa, A.; Takamura, H.; Okada M. Protium absorption properties and protide formations of Ti-Cr-V alloys. *J. Alloys Compd.* **2003**, *356–357*, 505–509.
3. Young, K.; Fetcenko, M.A.; Ouchi, T.; Im, J.; Ovshinsky, S.R.; Li, F.; Reinhout, M. Hydrogen Storage Materials Having Exunit cellent Kinetics, Capacity, and Cycle Stability. U.S. Patent 7,344,676, 18 March 2008.
4. Akiba, E.; H. Iba. Hydrogen absorption by Laves phase related BCC solid solution. *Intermetallics* **1998**, *6*, 461–470.
5. Cho, S.; Han, C.; Park, C.; Akiba, E. The hydrogen storage characteristics of Ti–Cr–V alloys. *J. Alloys Compd.* **1999**, *288*, 294–298.
6. Kuriwa, T.; Tamura, T.; Amemiya, T.; Fusa, T.; Kamegawa, A.; Takemura, T.; Okada, M. New V-based alloys with high protium absorption and desorption capacity. *J. Alloys Compd.* **1999**, *293–295* 433–436.
7. Seo, C.; Kim, J.; Lee, P.S.; Lee. J. Hydrogen storage properties of vanadium-based b.c.c. solid solution metal hydrides. *J. Alloys Compd.* **2003**, *348*, 252–257.
8. Tamura, T.; Tominaga, Y.; Matsumoto, K.; Fuda, T.; Kuriiwa, T.; Kamegawa, A.; Takamura, H.; Okada, M. Protium absorption properties of Ti-V-Cr-Mn alloys with a b.c.c. structure. *J. Alloys Compd.* **2002**, *330–332*, 522–525.

9. Huang, T.; Wu, Z,; Chen, J.; Yu, X.; Xia, B.; Xu, N. Dependence of hydrogen storage capacity of $TiCr_{1.8-x}(VFe)_x$ on V-Fe content. *Mat. Sci. Engineer. A.* **2004**, *385*, 17–21.
10. Yu, X.B.; Wu, Z.; Xia, B.J.; Xu, N.X. Enhancement of hydrogen storage capacity of Ti–V–Cr–Mn BCC phase alloys. *J. Alloys Compd.* **2004**, *372*, 272–277.
11. Hang, Z.; Xiao, X.; Tan, D.; He, Z.; Li, W.; Li, S.; Chen, C.; Chen, L. Microstructure and hydrogen storage properties of $Ti_{10}V_{84-x}Fe_6Zr_x$ (x = 1–8) alloys. *Int. J. Hydrogen Energy* **2010**, *35*, 3080–3086.
12. Liu, X.; Jiang, L.; Li, Z.; Huang, Z.; Wang, S. Improve plateau property of $Ti_{32}Cr_{46}V_{22}$ BCC alloy with heat treatment and Ce additive. *J. Alloys Compd.* **2009**, *471*, L36–L38.
13. Chen, X.; Yuan, Q.; Madigan, B.; Xue, W. Long-term corrosion behavior of martensitic steel welds in static molten Pb–17Li alloy at 550°C. *Corros. Sci.* **2015**, *96*, 178–185.
14. Chuang, H.J.; Huang, S.S.; Ma, C.Y.; Chan, S.L.I. Effect of annealing heat treatment on an atomized AB_2 hydrogen storage alloy. *J. Alloys Compd.* **1999**, *285*, 284–291.
15. Hang, Z.; Xiao, X.;Li, S.; Ge, H.; Chen, C.; Chen L. Influence of heat treatment on the microstructure and hydrogen storage properties of $Ti_{10}V_{77}Cr_6Fe_6Zr$ alloy. *J. Alloys Compd.* **2012**, *529*, 128–133.
16. Yu, X.B.; Wu, Z.; Xia, B.J.; Xu, N.X. A Ti-V-based bcc phase alloy for use as metal hydride electrode with high discharge capacity. *J. Chem. Phys.* **2004**, *121*, 987–990.
17. Young, K.; Ouchi, T.; Huang, B.; Nei, J. Structure, hydrogen storage, and electrochemical properties of body-centered-cubic $Ti_{40}V_{30}Cr_{15}Mn_{13}X_2$ alloys (*X* = B, Si, Mn, Ni, Zr, Nb, Mo, and La). *Batteries* **2015**, 1, 74–90.
18. Young, K.; Huang, B.; Regmi, R.K.; Lawes, G.; Liu, Y. Comparisons of metallic clusters imbedded in the surface oxide of AB_2, AB_5, and A_2B_7 alloy. *J. Alloys Compd.* **2010**, *506*, 831–840.
19. Young, K.; Ouchi, T.; Koch, J.; Fetcenko, M.A. Compositional optimization of vanadium-free hypo-stoichiometric AB_2 metal hydride alloy for Ni/MH battery application. *J. Alloys Compd.* **2012**, *510*, 97–106.
20. Young, K.; Ouchi, T.; Huang, B.; Fetcenko, M.A. Effects of B, Fe, Gd, Mg, and C on the structure, hydrogen storage, and electrochemical properties of vanadium-free AB_2 metal hydride alloy. *J. Alloys Compd.* **2012**, *511*, 242–250.
21. ASTM, Standard Practice for Calculation of Corrosion Rates and Related Information from Electrochemical Measurements, 1999, ASTM: West Conshohocken, United States.
22. Handzlik, P.; Fitzner, K. Corrosion resistance of Ti and Ti–Pd alloy in phosphate buffered saline solutions with and without H_2O_2 addition. *Tran. Nonfer. Met. Soc. China* **2013**, *23*, 866–875.
23. Young, K.; Nei, J. The current status of hydrogen storage alloy development for electrochemical application. *Materials* **2013**, *6*, 4574–4608.
24. Cho, S.; Enoki, H.; Akiba, E. Effect of Fe addition on hydrogen storage characteristics of $Ti_{0.16}Zr_{0.05}Cr_{0.22}V_{0.57}$ alloy. *J. Alloys Compd.* **2000**, *307*, 304–310.
25. Dou, T.; Wu, Z.; Mao, J.; Xu, N. Application of commercial ferrovanadium to reduce cost of Ti–V-based BCC phase hydrogen storage alloys. *Mater. Sci. Eng. A* **2008**, *476*, 34–38.
26. Santos, S.F.; Huot, J. Hydrogen storage in $TiCr_{1.2}(FeV)x$ BCC solid solutions. *J. Alloys Compd.* **2009**, *472*, 247–251.
27. Chen, N.; Li, R.; Zhu, Y.; Liu, Y.; Pan, H. Electrochemical hydrogenation and dehydrogenation mechanisms of the Ti–V base multiphase hydrogen storage electrode alloy. *Acta Metall. Sin.* **2004**, *40*, 1200–1204.
28. Young, K.; Ouchi, T.; Nei, J.; Wang, L. Annealing effects on Laves phase-related body-centered-cubic solid solution metal hydride alloys. *J. Alloys Compd.* **2016**, *654*, 216–225.
29. Ashworth, M.A.; Davenport., A.J.; Ward, R.M.; Hamilton, H.G.C. Microstructure and corrosion of Pd-modified Ti alloys produced by powder metallurgy. *Corros. Sci.* **2010**, *52*, 2413–2421.
30. Cho, S.-W.; Enokib, E.; Akibab, E. Effect of Fe addition on hydrogen storage characteristics of $Ti_{0.16}$ $Zr_{0.05}$ $Cr_{0.22}$ $V_{0.57}$ alloy. *J. Alloys Compd.* **2000**, *307*, 304–310.
31. Yoo, J.; Shim, G.; Cho, S.; Park, C. Effects of desorption temperature and substitution of Fe for Cr on the hydrogen storage properties of alloy. *Int. J. Hydrogen Energy* **2007**, *32*, 2977–2981.
32. Dou, T.; Wu, Z.; Mao, J.; Xu, N. Application of commercial ferrovanadium to reduce cost of Ti–V-based BCC phase hydrogen storage alloys. *Mat. Sci. Engineer. A.* **2008,** *476*, 34–38.

33. Itoh, H.; Arashima, H.; Kubo, K.; Kabutomori, T. The influence of microstructure on hydrogen absorption properties of Ti–Cr–V alloys. *J. Alloys Compd.* **2002**, *330*, 287–291.
34. Towata, S.; Noritake, T.; Itoh, A.; Aoki, M.; Miwa, K. Effect of partial niobium and iron substitution on short-term cycle durability of hydrogen storage Ti–Cr–V alloys. *Int. J. Hydrogen Energy* **2013**, *38*, 3024–3029.
35. Zhou, Y.; Chen, J.; Xu, Y.; Liu, Z. Effects of Cr, Ni and Cu on the Corrosion Behavior of Low Carbon Microalloying Steel in a Cl^- Containing Environment. *J. Mater. Sci. Tech*. **2013**, *29*, 168–174.
36. Kamimura, T.; Stratmann, M. The influence of chromium on the atmospheric corrosion of steel. *Corros. Sci.* **2001**, *43*, 429–447.
37. Shih, C.; Shih, C.; Su, Y.; Su, L.H.L.; Chang, M.; Lin, S. Effect of surface oxide properties on corrosion resistance of 316L stainless steel for biomedical applications. *Corros. Sci.* **2004**, *46*, 427–441.
38. Güleryüz, H.; H. Çimenoğlu. Effect of thermal oxidation on corrosion and corrosion–wear behaviour of a Ti–6Al–4V alloy. *Biomaterials* **2004**, *25*, 3325–3333.
39. Shi, P.; Ng, W.F.; Wong, M.H.; Cheng, F.T. Improvement of corrosion resistance of pure magnesium in Hanks' solution by microarc oxidation with sol–gel TiO_2 sealing. *J. Alloys Compd.* **2009**, *469*, 286–292.
40. Iba, H; Akiba, E. The relation between microstructure and hydrogen absorbing property in Laves phase-solid solution multiphase alloys. *J. Alloys Compd.* **1995**, *231*, 508–512.
41. Tsukahara, M.; Takahashi, K.; Mishima, T.; Isomura, A.; Sakai, T. V-based solid solution alloys with Laves phase network: hydrogen absorption properties and microstructure. *J. Alloys Compd.* **1996**, *236*, 151–155.